Overexpression of the short endoglin isoform reduces renal fibrosis and inflammation after unilateral ureteral obstruction

José M. Muñoz-Félix[a,b,*,1,2], Lucía Pérez-Roque[a,b,1], Elena Núñez-Gómez[a,b,1], Bárbara Oujo[a,b], Miguel Arévalo[c], Laura Ruiz-Remolina[a,b], Cristina Cuesta[a,b], Carmen Langa[d], Fernando Pérez-Barriocanal[a,b], Carmelo Bernabeu[d], José M. Lopez-Novoa[a,b]

[a]Renal and Cardiovascular Research Unit, Department of Physiology and Pharmacology, University of Salamanca, 37007 Salamanca, Spain

[b]Biomedical Research Institute of Salamanca (IBSAL), 37007 Salamanca, Spain

[c]Department of Human Anatomy and Histology, Universidad de Salamanca, 37007 Salamanca, Spain

[d]Centro de Investigaciones Biológicas, Consejo Superior de Investigaciones Científicas (CSIC), and Centro de Investigación Biomédica en Red de Enfermedades Raras (CIBERER), Madrid, Spain

[1]These authors have contributed equally to this work.

[2]Present address: Centre for Tumour Biology, Barts Cancer Institute, Queen Mary University of London, John Vane Science Centre, Charterhouse Square, London EC1M 6BQ, UK.

*Corresponding author: José M. Muñoz-Félix, Department of Physiology and Pharmacology; University of Salamanca, Edificio Departamental, Campus Miguel de Unamuno, 37007 Salamanca, Spain.

E-mail addresses: jmmb@usal.es, j.munoz-felix@qmul.ac.uk (J.M. Muñoz-Félix).

ABSTRACT

Transforming growth factor beta 1 (TGF-β1) is one of the most studied cytokines involved in renal tubulo¬interstitial fibrosis, which is characterized by myofibroblast abundance and proliferation, and high buildup of extracellular matrix in the tubular interstitium leading to organ failure. Endoglin (Eng) is a 180-kDa homodimeric transmembrane protein that regulates a great number of TGF-β1 actions in different biological processes, includ¬ing ECM synthesis. High levels of Eng have been observed in experimental models of renal fibrosis or in biopsies from patients with chronic kidney disease. In humans and mice, two Eng isoforms are generated by alternative splicing, L-Eng and S-Eng that differ in the length and composition of their cytoplasmic domains. We have previously described that L-Eng overexpression promotes renal fibrosis after unilateral ureteral obstruction (UUO). However, the role of S-Eng in renal fibrosis is unknown and its study would let us analyze the possible function of the cytoplasmic domain of Eng in this process. For this purpose, we have generated a mice strain that overexpresses S-Eng (S-ENG+) and we have performed an UUO in S-ENG+ and their wild type (WT) control mice. Our results indicate that obstructed kidney of S-ENG+ mice shows lower levels of tubulo-interstitial fibrosis, less inflammation and less interstitial cell proliferation than WT littermates. Moreover, S-ENG+ mice show less activation of Smad1 and Smad2/3 pathways. Thus, S-Eng overexpression reduces UUO-induced renal fibrosis and some associated mechanisms. As L-Eng overexpression provokes renal fibrosis we conclude that Eng-mediated induction of renal fibrosis in this model is dependent on its cytoplasmic domain.

Keywords: Fibrosis, Endoglin, TGF-β, Kidney, Animal model, Obstructive nephropathy

ABBREVIATIONS

α-SMA, α-smooth muscle actin

ALK1, activin receptor-like kinase 1

ALK5, activin receptor-like kinase 5

ANOVA, analysis of variance

ECM, extracellular matrix

Eng, endoglin

ICAM-1, intercellular cell adhesion molecule-1

NO, non-obstructed

O, obstructed

PDGF, Platelet-Derived Growth Factor

SEM, standard error of the mean

TGF-β1, transforming growth factor-β1

VCAM-1, vascular cell adhesion molecule-1

UUO, unilateral ureteral obstruction

WT, wild type

1. INTRODUCTION

Renal fibrosis is a process in which kidney structure and function are progressively altered because of the excessive deposition of extracellular matrix (ECM) components in both glomeruli (glomerulosclerosis) and interstitium (tubulo-interstitial fibrosis). Progressive tubule-interstitial fibrosis is the final common pathway for all kidney diseases, leading to chronic renal failure. The level of tubule-interstitial fibrosis is directly related to the impairment of renal function [1]. The histopathology of tubule-interstitial fibrosis is characterized by infiltration of inflammatory cells, tubular cell loss, fibroblasts accumulation, deposition of interstitial matrix, and rarefaction of the peritubular microvasculature. Inflammatory and other renal cells release to the interstitium different cytokines such as Transforming Growth Factor β (TGF-β) or Platelet-Derived Growth Factor (PDGF) that are involved in myofibroblast activation and accumulation [2]. TGF-β1 is one of the three TGF-β isoforms (named 1-3) present in mammals. The role of TGF-β1 as key molecule in the development of fibrosis and inflammation has been widely described [3–5]. TGF-β1 signaling pathway starts when TGF-β1 binds to its receptor type II (TβRII) which recruits the corresponding TGF-β type I receptor (TβRI). Two different type I receptors, named Activin receptor-Like Kinase 1 and 5 (ALK1 and ALK5 respectively), can be recruited by TβRII. Once the heterocomplex is formed, several Smad proteins are phosphorylated depending of the type I receptor recruited, and then translocated into the nucleus to produce the corresponding cell response. Thus, ALK1 recruitment leads to Smad1/5/8 phosphorylation whereas ALK5 complexing promotes Smad2/3 phosphorylation [6].

Endoglin (Eng) is a glycosylated transmembrane protein which is mainly expressed in endothelial cells [7], although it is also detected in other cell types such as macrophages [8], mesangial cells [9] or fibroblasts from fibrotic tissue [10,11]. Eng is a TGF-β1 co-receptor that participates in TGF-β1 signaling, and many studies have addressed the involvement of Eng in several fibrotic processes [11-16].Eng is overexpressed in kidneys of patients with chronic kidney disease [17] and in kidneys of animals with several experimental models of renal fibrosis [15]. Alternative splicing of human and mice Eng genes generates two mRNA that encode for two different isoforms of the protein named L-Eng (large) and S-Eng (short), according to the different lengths of their cytoplasmic tails [18,19]. It has been described that L-and S-Eng differentially modulate the TGF-β1 signaling pathway [20,21]. A previous study from our group demonstrated that L-Eng over-expression increases renal fibrosis after unilateral ureteral obstruction (UUO) [16]. However, the individual role of S-Eng in renal fibrosis is still unknown. Thus, the aim of the present study was to determine the effect of S-Eng overexpression in renal fibrosis and whether its much shorter cytoplasmic tail affects TGF-β1 signaling in this process. For this purpose, we used a mice transgenic for S-Eng and a widely used experimental model of obstructive nephropathy and renal fibrosis, the UUO [22].

Our results show that S-Eng overexpression counteracts TGF-β-induced renal fibrosis. As L-Eng promotes renal fibrosis and TGF-β-in¬duced signaling pathways during renal fibrosis, we conclude that the cytoplasmic tail of Eng is involved in TGF-β-induced renal fibrosis.

2. MATERIAL AND METHODS

2.1. Generation and characterization of S-ENG+ transgenic mice

To generate a transgenic mice expressing human S-Eng (S-ENG+), HA-tagged L-Eng-pCAGGS [16] and S-Eng cDNA [18] in pCDH (System Biosciences) were used to derive the S-Eng-pCAGGS construct. The pCDH-S-Eng was digested with NotI and the obtained Eng fragment was inserted into the L-Eng-pCAGGS plasmid previously digested with NotI. The resulting S-Eng-pCAGGS vector encodes the Eng leader sequence (amino acids 1-25) followed by the influenza hemagglutinin epitope (HA; Tyr-Pro-Tyr-Asp-Val-Pro-Asp-Tyr-Ala) and the mature S-Eng (variant 2, amino acids 26-625). The S-Eng-pCAGGS plasmid is under the control of a ubiquitous actin promoter [16].The pCAGGS plasmid contains, from 5′ to 3′, a CMV enhancer, a chicken enhancer and promoter, a β-globin intron, an EcoRI site, and a β-globin polyadenylation motif. To obtain linear DNA fragments for microinjec¬tion, the expression vector S-Eng-pCAGGS was digested with SalI/KpnI and the Eng containing 5.0-kb fragment was separated by agarose gel electrophoresis. The purified fragment (Fig. 1a) was microinjected into CBAxC57BL/6J fertilized eggs at the University of Salamanca Transgenic Facility, using standard protocols. Progeny was screened for Eng transgene by PCR of tail DNA using forward (5′-AGAGCATCCTCCTCCG ACTGG-3′) and reverse (5′-TGAAGCCACGAATGTTTTTCT-3′)primers. S-ENG+ transgenic founders were crossed with C57BL/6J mice to perpetuate the transgenic lines. Mice were kept in a pathogen-free facility for genetically modified animals (Servicio de Experimentación Animal, SEA; University of Salamanca).

2.2. Mice and animal disease

All studies were performed in parallel in S-ENG+ and WT male mice aged 8 weeks. UUO procedure was performed as previously described [12,23]. In brief, mice were anesthetized with Isoflurane (Schering-Plough, Madrid, Spain), the abdomen was opened and the left ureter was located and occluded in two places with 5-0 silk. The abdomen was closed with running suture and the skin was closed with interrupted sutures. After surgery, animals were kept warm during 3 h and a single dose of analgesic (Buprenorphine, Schering-Plough, Madrid, Spain) was injected subcutaneously to reduce pain in the post-surgery phase. Sham-operated (SO) animals were included as controls. Subsequently, mice were housed in a temperature-controlled room with a 12 h light/dark cycle and fed on standard chow (Panlab, Barcelona, Spain) and water ad libitum. UUO was maintained during 15 days. All the studies were approved by the Animal Care and Use Committees of the University of Salamanca and mice were cared in compliance with the rules of European

Union and with the US Department of Health and Human Services Guide for the Care and Use of Laboratory Animals.

2.3. Blood pressure measurement

Blood pressure was recorded in conscious mice with an automated multichannel system by using the tail-cuff method and a photoelectric sensor (Niprem 546; Cibertec, Madrid, Spain). Animals were previously accustomed for several days and measures were collected at the same hour during at least 3 days.

2.4. Renal function measurement

Before UUO, mice were placed in metabolic cages and urine was collected in 24 h periods. Plasma and urine creatinine (CrP and CrU, respectively) were measured using a commercial kit (Quantichrom™, BioAssay Systems). The assay was carried out according to manufacturer's instructions. Creatinine clearance (ClCr) was calculated: CrU × 24-h urine output × CrP^{-1}. Urine protein concentration was measured using the Bradford method.

2.5. ELISA

Plasma concentrations of human soluble endoglin (Sol-Eng) were determined by using the Quantikine® ELISA kit for Human Endoglin/ CD105 (R&D Systems).

2.6. Histology

Histological studies were performed in 4 S-ENG+ and 4 WT animals subjected to UUO, and 4 S-ENG+ and 4 WT animals subjected to sham-operation. Fifteen days after UUO or sham-operation, animals were anesthetized with Pentobarbital and perfused with heparinized saline solution. In each animal, both kidneys were removed, halved longitudinally and fixed in 4% buffered formalin for 24 h. Subsequently, kidneys were dehydrated in ascending series of ethanol, cleared in xylene and embedded in paraffin. Kidney sections (3 µm) were stained either for haematoxylin-eosin or Masson's trichrome for light microscopy analysis.

2.7. Morphometric studies

Additional 5 µm thick renal sections were cut mounted on glass slides and stained with Sirius red (Direct Red 80, Sigma-Aldrich Quimica, Madrid, Spain) to evaluate the area occupied by collagen fibres. From each kidney, a total of 15 interstitial images of each slide were captured and processed with a high-resolution video camera (Sony, DF-W-X710) connected to a light microscope (Nikon Eclipse 50i) using the 20× objective and a green optical filter (IF 550). The area occupied by collagen was measured using a computerized image analy¬sis system (Fibrosis HRR, Master Diagnóstica) as previously described [24]. The values obtained were expressed in square micrometers. The possible differences in tubular damage between S-ENG+ vs. WT were assessed in sections stained with haematoxylin/eosin. From each preparation five widely separated images

were digitalized and the total area of the tubular lumen was analyzed by using an image analysis system and a specific software [25].

2.8. Immunohistochemical studies

3 µm sections were processed for immunohistochemistry as follows. Sections were deparaffined in xylene and rehydrated in graded ethanol. Endogenous peroxidase was blocked with 3% hydrogen peroxide, followed by primary antibody incubation. Primary antibodies are specified in Table 1. Then, sections were washed three times in PBS and incubated with the Novolink Polymer Detection System (Novocastra, MA, USA), followed by reaction with 3,3'-diaminobenzidine as chromogen. Negative WT slides were prepared without primary antibody, as negative controls for antibody specificity. Ten images per slide were digitalized and processed with the same video camera and microscope described for the analysis of fibrosis. The number of positive cells was quantified by using ImageJ software (Rasband, W.S., ImageJ, National Institutes of Health, Bethesda, Maryland, USA).

2.9. Rarefaction study

Quantification of peritubular capillaries (PTC) loss was performed by calculating the rarefaction index as previously described [26]. Briefly, the CD31-immunostained sections were examined across a 10 × 10 grid under a ×40 objective. Each square within the grid that did not contain CD31-positive capillaries was counted. 5 fields in the cortex and outer medulla were examined on the cross-section of each kidney, and a mean score per section was calculated. This scoring system, thus, inversely reflects PTC rarefaction, whereby low values represent intact capillaries and higher values indicate loss of capillaries (the minimum possible capillary score is 0, and the maximum score is 100).

2.10. Western blot analysis

For Western blot, SO, NO, O kidneys were removed from wild type and S-ENG+ mice [WT: SO (n =6); NO (n =8); O(n = 8) and S-ENG+:SO (n = 6); NO (n =8); O(n = 8)] and immediately stored at -80 °C. Tissue protein extracts were prepared as previously described [16]. Total kidney protein lysates (60 µg) were fractioned by SDS¬PAGE, transferred onto PVDF membrane (Millipore Billerica, MA, USA) and incubated overnight at 4 °C with the antibodies for endoglin, fibronectin, collagen I, α-SMA, PCNA, Smad1, Smad2/3, phospho-Smad1, phospho-Smad3, ICAM-1, VCAM-1, COX-2, GAPDH, β-actin, ALK1 and ALK5 in the conditions specified in Table 2. Development was performed using a chemiluminescent reagent (ECL detection reagent, Amersham Biosciences) and signals were recorded on X-ray film (Fujifilm), followed by densitometric analysis (Scion Image).

After considering various molecules as loading controls, it was observed that UUO induced expression changes in all of them. Therefore, GAPDH was used to assess loading, but not quantified neither used for

protein expression relativization. Moreover, reblotting was necessary for Smad1 and pSmad1, and for pSmad2 and Smad2/3.

2.11. PCR analysis

For RT-PCR analysis, total RNA was isolated using Nucleospin RNAII (Macherey-Nagel), according to the manufacturer's instructions. Single-strand cDNA was generated from 250 ng of total RNA using iScript RT Supermix (Bio-Rad). Quantitative PCR was performed in triplicate. Each 20 µl reaction contained 1 µl of cDNA, 400 nM of each primer, and 1× iQ SybrGreen Supermix (Bio-Rad). Standard curves were run for each transcript to ensure exponential amplification and to rule out non-specific amplification. Primers used were: For mouse Eng: forward 5'-GACTTCAGATTGGAATACCTTGG-3' and reverse 5'-CAGTGCCGTGTCTTTCTGTAAT-3'. 95°C, 5 min;40 cycles of 30s, 95°C, 30 s, 59 °C and 30 s, 72 °C. Gene expression was normalized to RPS13 expression. The reactions were run on an iQ5 Real-time PCR detection system (Bio-Rad).

2.12. Statistical analysis

Data are expressed as mean ± standard error of the mean (SEM). Comparison of means was performed by two-way analysis of variance (ANOVA). Statistical differences between groups were assessed by the Bonferroni test and by the Student t-test. Data were analyzed using the GraphPad Prism 6. A p value lower than 0.05 was considered statistically significant.

3. RESULTS

3.1. Characterization of transgenic mice

We generated a transgenic mice expressing human S-Eng (S-ENG+) under the control of a ubiquitous actin promoter (Fig. 1a). A breeding colony of adult S-ENG+ animals has been maintained in our facilities for N2 years. Studies were performed in the third generation of backcrossing. The S-ENG+ transgenic mice show normal growth and reproductive patterns (data not shown). Expression of human S-Eng was detected in heart, lung, spleen, kidney and liver (Fig. 1b). We proved that human endoglin is expressed in sham-operated (SO), non-obstructed (NO) and obstructed (O) kidneys from S-ENG+ mice (Fig. 1c). S-ENG+ animals show similar arterial pressure, and renal function (assessed by creatinine clearance and proteinuria) than WT mice (Fig. 1d). We observed high levels of plasmatic human Sol-Eng in S-ENG+ mice, that is absent from WT mice (Fig. 1e).

3.2. Renal endoglin expression after UUO

PCR studies demonstrated that murine Eng expression was marked¬ly higher in the O kidney than in the NO kidney in WT mice subjected to UUO. However, mouse S-Eng expression was similar in O and NO kidneys (Fig. 1f). This suggests that total Eng increase in O kidneys can be attributed to an increase in L-Eng levels.

Renal TGF-β levels were also found higher in O than in NO kidneys and no significant differences were observed between S-ENG+ and control mice (Fig. 1g).

The amount of TGF-beta type I receptor ALK1 was higher (although the difference was not statistically significant) in the O than in the NO kidneys, without differences between WT and S-ENG+ mice (Fig. 1h, upper panel). ALK5 showed no differences between O and NO kidneys both in WT and in S-ENG+ mice (Fig. 1h, lower panel).

3.3. Structural kidney alterations after UUO

SO kidneys from S-ENG+ or WT mice exhibited morphological alterations. In contrast, O kidneys from both mouse strains showed typical features of hydronephrosis, including medullar compression towards cortex, flattening of both inner medulla and papillae, tubular dilation and flattened epithelium in affected tubules (Fig. 2a). When additional slides were stained with Masson's trichrome, a higher amount of fibrous tissue in O compared with NO kidneys was observed. The extension of fibrotic tissue was higher in WT than in S-ENG+ animals (Fig. 2b). Furthermore, a quantitative study of fibrosis extension was performed in sections stained with Sirius red. Thus, computer assisted analysis showed a significantly higher fibrosis area in O kidneys from WT than in those from S-ENG+ animals (Fig. 2c). No manifest structural alterations or fibrosis were detected in NO kidneys or in SO kidneys from WT or S-ENG+ (Fig. 2).

3.4. S-Eng overexpressing mice have reduced renal collagen I and fibronectin contents after UUO

Renal levels of collagen I and fibronectin, two major components of extracellular matrix, were also assessed by immunohistochemistry and Western blot analysis. Collagen I and fibronectin contents were very low in NO kidneys and in SO kidneys from WT or S-ENG+ mice, whereas the expression of both proteins was higher in O kidneys from WT than in those from S-ENG+ mice (Fig. 3a). In agreement with the immunohisto¬chemistry data, we observed by Western blot analysis that the content of collagen I and fibronectin was significantly higher in O than in NO kidneys from WT and S-ENG+ mice. The amount of both proteins was significantly lower in O kidneys from S-ENG+ animals than in O kidneys from WT animals (Fig. 3b). These results suggest that S-Eng overexpres¬sion decreases UUO-induced ECM protein accumulation.

3.5. S-Eng overexpressing mice reduce renal myofibroblast abundance after UUO

A typical feature of the fibrotic kidney is the activation and prolifer¬ation of myofibroblasts in the renal interstitium, being these cells a major source of ECM proteins [27,28].Myofibroblast abundance in the kidney can be assessed by the accumulation of two markers, α-smooth muscle actin (α-SMA) and fibroblast specific protein-1 or S100A4 [29]. Immunohistochemistry analysis for α-SMA (Fig. 4a) and S100A4 (Fig. 4b) revealed a higher staining of both proteins in O kidneys than in NO kidneys. Immunostaining for both α-SMA and S100A4 was lower in O kidneys from S-ENG+ than in those from WT mice.

S100A4 protein content, assessed by Western blot, was also higher in O than in NO kidneys, after UUO, and this content was slightly lower in O kidneys from S-ENG+ mice compared with those from WT animals (Fig. 4c).

3.6. Effect of S-Eng overexpression on the proliferation of renal cells after UUO

The number of proliferating renal cells was assessed by counting nuclear immunostaining of Ki67, whose expression is strictly associated with the proliferative process. NO and SO kidneys presented scarce positive Ki67-possitive nuclei in both tubules and interstitium. O kidneys from WT animals showed a significantly higher number of Ki67 stained tubular and interstitial cell nuclei than those from S-ENG+ mice (Fig. 5a). By a separate analysis of Ki67-possitive tubular cells and Ki67-positive interstitial cells, we show that both tubular and interstitial Ki67 cells are in a lower quantity in O kidneys from WT and S-ENG+ mice (Fig. 5b).

To confirm these results, we analyzed the expression of proliferation cell nuclear antigen (PCNA) by Western blot. PCNA expression was higher in O than in NO kidneys after UUO in WT and S-ENG+ mice. PCNA content was lower in O kidneys from S-ENG+ than in those from WT mice (Fig. 5c). On the other hand, tubular damage (evaluated by tubular lumen area) was lower in O kidneys from S¬ENG+ than in those from WT mice (Fig. 5d).

3.7. S-Eng overexpression reduces inflammation after UUO

Inflammatory cell infiltration is one of the key processes that contribute to the establishment of tubulo-interstitial fibrosis [1,30].To evaluate if S-Eng also modifies the UUO-induced renal inflammation process, we analyzed the expression of molecule characteristics of in¬flammatory cells such as CD68 (a marker of monocytes/macrophages), COX-2 or iNOS (expressed by inflammatory cells) and those involved in cell infiltration such as intercellular cell adhesion molecule-1 (ICAM-1) and vascular cell adhesion molecule-1 (VCAM-1).

Immunostaining showed the presence of numerous CD68-positive cells in the interstitium of O kidneys from WT or S-ENG+ animals (Fig. 6a). However, the amount of cells stained for CD68 was clearly lower in O kidneys from S-ENG+ than in those from WT mice. Few or no macrophages were detected in NO and SO kidneys from either geno¬type (Fig. 6a). Western blot quantification of cell adhesion molecules (CAMs) revealed a higher content in O kidneys than in NO or SO kidneys from mice of either genotype. The amount of ICAM-1 and VCAM-1 was slightly lower in O kidneys from S-ENG+ than in those from WT mice (Fig. 6b), although the difference did not reach statistical significance.

Immunohistochemistry for iNOS indicated a low number of cells stained in NO and SO kidneys, whereas a marked staining was observed in tubular and macrophage-like interstitial cells of O kidneys from both mice

genotypes. The cell staining of iNOS was clearly lower in O kidneys from S-ENG+ than in those from WT mice (Fig. 6a).

Western blot analysis showed that levels of COX-2 were negligible in NO and SO kidneys from both type of animals, but they were very high in O kidneys. COX-2 levels in O kidneys from S-ENG+ mice were significantly lower than in those from WT mice (Fig. 6b). Number of peritubular capillaries and small vessels (stained with CD31) decreased after UUO in WT and S-ENG+ mice, suggesting vascular rarefaction in the UUO model. However, this increase in vascular rarefaction was lower in O kidneys from S-ENG+ mice (Fig. 6c).

3.8. Effects of S-Eng overexpression in the TGF-β/Smad signaling pathway

To assess the effect of S-Eng on TGF-β/Smad signaling in this model of renal fibrosis, we evaluated Smad1, Smad2 and Smad3 phosphorylation by measuring the abundance of pSmad1, pSmad2 and pSmad3 protein levels by Western blot and by immunohistochemistry.

Activation of the Smad2/3 pathway has been widely associated to fibrosis in several organs [15]. Immunohistochemistry analysis revealed a weak nuclear expression of pSmad2/3 and pSmad1/5 in NO and sham animals (Figs. 7a, 8a). We also observed a higher number of nuclei positive for pSmad2/3 in O than in NO kidneys. The number of nuclei positive for pSmad2/3 was significantly lower in O kidneys from S-ENG+ than in kidneys from WT mice (Fig. 7a). Cells positive for pSmad1/5/8 were almost not detectable in SO or NO kidneys in both mice genotypes, whereas strong staining in many nuclei and, to a lesser extent, in cytoplasm was observed in O kidneys. The number of cells positive for pSmad1/5 in O kidneys from S-ENG+ was much lower than that observed in O kidneys from WT (Fig. 8a).

Similar results were obtained measuring the abundance of pSmads by Western blot. pSmad 2 and 3 abundance was much higher in O than in NO kidneys, and their abundance was significantly lower in O kidneys from S-ENG+ than in O kidneys from WT mice. Total amount of Smad2/3 was similar in O and NO groups from both genotypes of mice (Fig. 7b). The levels of pSmad1, assessed by Western blot analysis, were also higher in O than in NO kidneys, being lower (although not significant) in the O kidneys from S-ENG+ than in O kidneys from WT mice (Fig. 8b). Surprisingly, total Smad1 levels were also lower in O than in NO kidneys in both S-ENG+ and WT mice (Fig. 8b).

4. DISCUSION

Eng is expressed in many profibrogenic cells as mesangial cells and renal fibroblasts of the kidney, as well as in skin, intestinal and cardiac fibroblasts, and in cultured portal fibroblasts and hepatic stellate cells of the liver [14,31]. Eng upregulation has been observed in several experimental models of renal fibrosis [12,32]. In agreement with these reports, our present data in the UUO model of tubulo-interstitial fibrosis shows the

increase in both Eng mRNA and protein expression in the O kidney (Fig. 1). Several authors demonstrated that Eng promotes fibrosis in different kidney experimental models [15,16,33-37] and other experimental models of tissue fibrosis in organs such as heart [13,38], liver [39] or skin [40]. Two different Eng isoforms that differ exclusively in the intracellular tail have been reported in both humans [18] and mice [19]. Recently, our laboratory described that overexpression of L-Eng, the predominant isoform, promotes renal fibrosis in the UUO model, via increasing Smad1 and Smad3 phosphorylation [16].However, the possible role of S-Eng in renal fibrosis has not been assessed. Hence, our aim was to elucidate the possible function of this isoform in the fibrogenic process of the kidney subjected to UUO.

Our results demonstrate for the first time that overexpression of the short isoform of Eng is associated to a significant reduction of ECM protein synthesis and accumulation in the obstructed kidney following UUO. Reduced levels of α-SMA and S100A4 in these kidneys suggest that the overexpression of S-Eng leads to a reduced abundance of myofibroblasts. On the other hand, myofibroblast and tubular epithelial cell proliferation is a common feature of UUO model [41].In this study we have detected that Ki67 and PCNA expression was higher in the O than in the NO kidneys in both WT and S-ENG+ mice, but this expres¬sion was lower in the O kidneys of S-ENG+ than in those from WT mice. Proliferation and differentiation of resident fibroblast are currently considered as the main sources of myofibroblasts in the renal interstitium during fibrosis [42,43]. The amount of Ki67 positive interstitial nuclei, most probably corresponding to myofibroblasts, was lower in S-ENG+ than in WT mice. Our data suggest that S-Eng overexpression counteracts myofibroblast proliferation and abundance after UUO.

Vascular rarefaction and consequent tissular hypoxia is one of the main features of renal fibrosis [44]. Our data also suggest that overexpression of S-ENG+ leads to a lower vascular rarefaction after UUO.

We have also observed in the O kidneys of S-ENG+, compared with those from WT mice, a lower amount of cells expressing CD68 (a marker of monocytes/macrophages), COX-2 (an enzyme characteristic of inflammatory cells), as well as a reduced iNOS protein amount. It should be noted that blood monocytes can migrate to sites of inflammation, differentiate into macrophages and induce inflammatory response lead¬ing to tubulointerstitial injury in renal inflammation in the UUO model of renal fibrosis [45]. Adhesion molecules such as ICAM-1 and VCAM-1 play a major role in monocyte macrophage infiltration into the kidneys [45]. The expression of these adhesion molecules was lower in the obstructed kidney of S-ENG+ compared with that from WT mice, although the difference was not significant. The involvement of Eng in inflammatory cell infiltration in experimental models of kidney damage has been already demonstrated [33,37]. Thus, all our data suggest a lower inflammatory status in the O kidneys from S-ENG+ mice compared with the O kidneys from WT mice, a fact that could contribute to the reduction in renal fibrosis observed in these animals.

TGF-β can exert its profibrotic effect through ALK5-Smad3 pathway activation [46,47], and phosphorylated Smad2 and Smad3 levels are increased after UUO [48-50]. In this study, we report a markedly lower Smad2 and Smad3 phosphorylation in O kidneys from S-ENG+ compared with those from WT mice, thus suggesting that the lower accumulation of ECM proteins, and hence, lower renal fibrosis observed in S-ENG+ mice, could be based in a lower activation of this signaling pathway in the presence of S-Eng.

On the other hand, Smad1 phosphorylation has been related with reversion of renal fibrosis, when it is activated by other cytokines such as bone morphogenic protein-7 (BMP-7) [51,52]. However, Smad1 phosphorylation also has been related to the fibrotic process in several organs such as skin [53], liver [54] and kidney [55]. It has been already described that renal levels of phospho-Smad1/5/8 increase after UUO [50]. In the present study, we demonstrate that the levels of Smad1 phosphorylation after UUO are lower in S-ENG+ than in WT mice, which suggest a role for the ALK1/Smad1 pathway in the generation of renal fibrosis in the kidney, as previously suggested [56].

We have also observed high levels of human Sol-Eng in serum from S-ENG+ mice, whereas human Sol-Eng was undetectable in plasma from WT animals. Sol-Eng is produced by proteolytic cleavage of the membrane isoform, releasing to the plasma almost all the extracellular part of the molecule. It can be suggested that increased plasma levels of Sol-Eng in S-ENG+ mice derive from the cleavage of the high levels of membrane human S-Eng. It is thought that Sol-Eng interacts with TGF-β molecules and thus prevents its interaction with the cell-surface endoglin [57–59]. However, this interaction has not been demonstrated clearly. It has been reported that Sol-Eng cannot directly scavenge TGF-β unless a complex of Sol-Eng-sTβRII is present [60,61] and that the ability of a recombinant Sol-Eng to block TGF-β1 and thus block its binding to cell surface receptors was very low compared with soluble TβRII [62]. Consequently, our hypothesis is that the high levels of Sol-Eng present in the serum of S-ENG+ mice do not interfere with the TGF-β pathway and the reduced fibrosis and inflammation after ureteral ligation observed in S-ENG+ mice are not due to the scavenging of TGF-β by Sol-Eng. However, one cannot rule out the possibility that Sol-Eng is present in circulation in a complex with soluble TβRII and even soluble TβRI that could scavenge TGF-β1 and blocked their effects on the renal cells.

As a conclusion, whereas L-Eng overexpression has been shown to promote both Smad1 and Smad2/3 phosphorylation, inflammation and renal fibrosis after UUO, we now demonstrate that S-Eng overexpression seems to inhibit these processes. As the only difference between these Eng isoforms is the intracellular domain, we postulate that this intracellular region plays a major role in the effect of Eng activating Smad2/3 and Smad1/5/8 phosphorylation, inflammatory cell infiltration and renal fibrosis after UUO (Fig. 9).

Disclosure

All the authors declared no competing interests

Acknowledgements

Authors wish to thank Ms Lucía Martin and Ms Annette Düwel for helping with animal breeding and Dr. Manuel Sanchez-Martín (Transgenic Mouse Facility) for the generation of transgenic mice. We also wish to thank Ms Angustias Pérez and Ms Marta Ortiz for their technical assistance in histology. This study has been supported by grants from Ministerio de Economía y Competitividad of Spain (SAF2013-43421-R to CB; and SAF2013-45784-R to JML-N), Junta de Castilla y León (GR100, JML-N), Institute Queen Sophie for Renal Research, Fundación Renal Íñigo Álvarez de Toledo, Madrid, Spain (0016¬002), Centro de Investigación Biomédica en Red de Enfermedades Raras (CIBERER, CB) (ISCIII-CB06/07/0038) and Red de Investigación Cooperativa en Enfermedades Renales (REDINREN, JML-N) (R12/0021/ 0032). CIBERER and REDINREN are initiatives of the Instituto de Salud Carlos III (ISCIII) of Spain supported by FEDER funds. BO and ENG are supported by fellowships from Ministerio de Economía y Competitividad (BES-2011-048968 and BES-2008-005550). JMMF, LPR and CC are supported by fellowships from Junta de Castilla y León and Fondo Social Europeo (EDU/1204/2010 and EDU/1083/2013).

REFERENCES

[1] M. Zeisberg, E.G. Neilson, Mechanisms of tubulointerstitial fibrosis, J. Am. Soc. Nephrol. 21 (2010) 1819-1834.

[2] P. Boor, T. Ostendorf, J. Floege, Renal fibrosis: novel insights into mechanisms and therapeutic targets, Nat. Rev. Nephrol. 6 (2010) 643-656.

[3] F.J. Lopez-Hernandez, J.M. Lopez-Novoa, Role of TGF-beta in chronic kidney disease: an integration of tubular, glomerular and vascular effects, Cell Tissue Res. 347 (2012) 141-154.

[4] D. Pohlers, J. Brenmoehl, I. Loffler, C.K. Muller, C. Leipner, S. Schultze-Mosgau, A. Stallmach, R.W. Kinne, G. Wolf, TGF-beta and fibrosis in different organs -molecular pathway imprints, Biochim. Biophys. Acta 1792 (2009) 746-756.

[5] X.M. Meng, A.C. Chung, H.Y. Lan, Role of the TGF-beta/BMP-7/Smad pathways in renal diseases, Clin. Sci. (Lond.) 124 (2013) 243-254.

[6] F. Lebrin, M. Deckers, P. Bertolino, P. Ten Dijke, TGF-beta receptor function in the endothelium, Cardiovasc. Res. 65 (2005) 599-608.

[7] A. Gougos, M. Letarte, Primary structure of endoglin, an RGD-containing glycoprotein of human endothelial cells, J. Biol. Chem. 265 (1990) 8361-8364.

[8] P. Lastres, T. Bellon, C. Cabanas, F. Sanchez-Madrid, A. Acevedo, A. Gougos, M. Letarte, C. Bernabeu, Regulated expression on human macrophages of endoglin, an Arg-Gly-Asp-containing surface antigen, Eur. J. Immunol. 22 (1992) 393-397.

[9] A. Rodriguez-Barbero, J. Obreo, N. Eleno, A. Rodriguez-Pena, A. Duwel, M. Jerkic, A. Sanchez-Rodriguez, C. Bernabeu, J.M. Lopez-Novoa, Endoglin expression in human and rat mesangial cells and its upregulation by TGF-beta1, Biochem. Biophys. Res. Commun. 282 (2001) 142-147.

[10] A. Leask, D.J. Abraham, D.R. Finlay, A. Holmes, D. Pennington, X. Shi-Wen, Y. Chen, K. Venstrom, X. Dou, M. Ponticos, C. Black, C. Bernabeu, J.K. Jackman, P.R. Findell, M.K. Connolly, Dysregulation of transforming growth factor beta signaling in scleroderma: overexpression of endoglin in cutaneous scleroderma fibroblasts, Arthritis Rheum. 46 (2002) 1857-1865.

[11] J.P. Burke, R.W. Watson, J.J. Mulsow, N.G. Docherty, J.C. Coffey, P.R. O'Connell, Endoglin negatively regulates transforming growth factor beta1-induced profibrotic responses in intestinal fibroblasts, Br. J. Surg. 97 (2010) 892-901.

[12] A. Rodriguez-Pena, N. Eleno, A. Duwell, M. Arevalo, F. Perez-Barriocanal, O. Flores, N. Docherty, C. Bernabeu, M. Letarte, J.M. Lopez-Novoa, Endoglin upregulation during experimental renal interstitial fibrosis in mice, Hypertension 40 (2002) 713-720.

[13] N.K. Kapur, S. Wilson, A.A. Yunis, X. Qiao, E. Mackey, V. Paruchuri, C. Baker, M.J. Aronovitz, S.A. Karumanchi, M. Letarte, D.A. Kass, M.E. Mendelsohn, R.H. Karas, Reduced endoglin activity limits cardiac fibrosis and improves survival in heart failure, Circulation 125 (2012) 2728-2738.

[14] S.K. Meurer, L. Tihaa, E. Borkham-Kamphorst, R. Weiskirchen, Expression and functional analysis of endoglin in isolated liver cells and its involvement in fibrogenic Smad signalling, Cell. Signal. 23 (2011) 683-699.

[15] J.M. Munoz-Felix, B. Oujo, J.M. Lopez-Novoa, The role of endoglin in kidney fibrosis, Expert Rev. Mol. Med. 16 (2014) e18.

[16] B. Oujo, J.M. Munoz-Felix, M. Arevalo, E. Nunez-Gomez, L. Perez-Roque, M. Pericacho, M. Gonzalez-Nunez, C. Langa, C. Martinez-Salgado, F. Perez-Barriocanal, C. Bernabeu, J.M. Lopez-Novoa, L-endoglin overexpression increases renal fibrosis after unilateral ureteral obstruction, PLoS One 9 (2014) e110365.

[17] P. Roy-Chaudhury, J.G. Simpson, D.A. Power, Endoglin, a transforming growth factor-beta-binding protein, is upregulated in chronic progressive renal disease, Exp. Nephrol. 5 (1997) 55-60.

[18] T. Bellon, A. Corbi, P. Lastres, C. Cales, M. Cebrian, S. Vera, S. Cheifetz, J. Massague, M. Letarte, C. Bernabeu, Identification and expression of two forms of the human transforming growth factor-beta-binding protein endoglin with distinct cytoplasmic regions, Eur. J. Immunol. 23 (1993) 2340-2345.

[19] E. Perez-Gomez, N. Eleno, J.M. Lopez-Novoa, J.R. Ramirez, B. Velasco, M. Letarte, C. Bernabeu, M. Quintanilla, Characterization of murine S-endoglin isoform and its effects on tumor development, Oncogene 24 (2005) 4450-4461.

[20] F.J. Blanco, M.T. Grande, C. Langa, B. Oujo, S. Velasco, A. Rodriguez-Barbero, E. Perez-Gomez, M. Quintanilla, J.M. Lopez-Novoa, C. Bernabeu, S-endoglin expression is induced in senescent endothelial cells and contributes to vascular pathology, Circ. Res. 103 (2008) 1383-1392.

[21] S. Velasco, P. Alvarez-Munoz, M. Pericacho, P.T. Dijke, C. Bernabeu, J.M. Lopez-Novoa, A. Rodriguez-Barbero, L-and S-endoglin differentially modulate TGFbeta1 signaling mediated by ALK1 and ALK5 in L6E9 myoblasts, J. Cell Sci. 121 (2008) 913-919.

[22] J.L. Bascands, J.P. Schanstra, Obstructive nephropathy: insights from genetically engineered animals, Kidney Int. 68 (2005) 925-937.

[23] M.T. Grande, I. Fuentes-Calvo, M. Arevalo, F. Heredia, E. Santos, C. Martinez-Salgado, D. Rodriguez-Puyol, M.A. Nieto, J.M. Lopez-Novoa, Deletion of H-Ras decreases renal fibrosis and myofibroblast activation following ureteral obstruction in mice, Kidney Int. 77 (2010) 509-518.

[24] A.M. Rodriguez-Lopez, O. Flores, M.A. Arevalo, J.M. Lopez-Novoa, Glomerular cell proliferation and apoptosis in uninephrectomized spontaneously hypertensive rats, Kidney Int. Suppl. 68 (1998) S36-S40.

[25] C.A. Schneider, W.S. Rasband, K.W. Eliceiri, NIH Image to ImageJ: 25 years of image analysis, Nat. Methods 9 (2012) 671-675.

[26] H.P. Gerber, K.J. Hillan, A.M. Ryan, J. Kowalski, G.A. Keller, L. Rangell, B.D. Wright, F. Radtke, M. Aguet, N. Ferrara, VEGF is required for growth and survival in neonatal mice, Development 126 (1999) 1149-1159.

[27] M.T. Grande, J.M. Lopez-Novoa, Fibroblast activation and myofibroblast generation in obstructive nephropathy, Nat. Rev. Nephrol. 5 (2009) 319-328.

[28] R.L. Chevalier, M.S. Forbes, B.A. Thornhill, Ureteral obstruction as a model of renal interstitial fibrosis and obstructive nephropathy, Kidney Int. 75 (2009) 1145-1152.

[29] F. Strutz, M. Zeisberg, Renal fibroblasts and myofibroblasts in chronic kidney disease, J. Am. Soc. Nephrol. 17 (2006) 2992-2998.

[30] M.T. Grande, F. Perez-Barriocanal, J.M. Lopez-Novoa, Role of inflammation in tubulo-interstitial damage associated to obstructive nephropathy, J. Inflamm (Lond) 7 (2010) 19.

[31] K.W. Finnson, A. Philip, Endoglin in liver fibrosis, J. Cell Commun. Signal. 6 (2012) 1-4.

[32] A. Rodriguez-Pena, M. Prieto, A. Duwel, J.V. Rivas, N. Eleno, F. Perez-Barriocanal, M. Arevalo, J.D. Smith, C.P. Vary, C. Bernabeu, J.M. Lopez-Novoa, Up-regulation of endoglin, a TGF-beta-binding protein, in rats with experimental renal fibrosis induced by renal mass reduction, Nephrol. Dial. Transplant. 16 (Suppl. 1) (2001) 34-39.

[33] N.G. Docherty, J.M. Lopez-Novoa, M. Arevalo, A. Duwel, A. Rodriguez-Pena, F. Perez-Barriocanal, C. Bernabeu, N. Eleno, Endoglin regulates renal ischaemia-reperfusion injury, Nephrol. Dial. Transplant. 21 (2006) 2106-2119.

[34] M. Scharpfenecker, B. Floot, N.S. Russell, P. Ten Dijke, F.A. Stewart, Endoglin haploinsufficiency reduces radiation-induced fibrosis and telangiectasia formation in mouse kidneys, Radiother. Oncol. 92 (2009) 484-491.

[35] M. Scharpfenecker, B. Floot, R. Korlaar, N.S. Russell, F.A. Stewart, ALK1 heterozygosity delays development of late normal tissue damage in the irradiated mouse kidney, Radiother. Oncol. 99 (2011) 349-355.

[36] M. Scharpfenecker, B. Floot, N.S. Russell, R.P. Coppes, F.A. Stewart, Endoglin haploinsufficiency attenuates radiation-induced deterioration of kidney function in mice, Radiother. Oncol. 108 (2013) 464-468.

[37] M. Scharpfenecker, B. Floot, N.S. Russell, F.A. Stewart, The TGF-beta co-receptor endoglin regulates macrophage infiltration and cytokine production in the irradiated mouse kidney, Radiother. Oncol. 105 (2012) 313-320.

[38] B.W. Wang, G.J. Wu, W.P. Cheng, K.G. Shyu, MicroRNA-208a increases myocardial fibrosis via endoglin in volume overloading heart, PLoS One 9 (2014) e84188.

[39] S.K. Meurer, M. Alsamman, H. Sahin, H.E. Wasmuth, T. Kisseleva, D.A. Brenner, C. Trautwein, R. Weiskirchen, D. Scholten, Overexpression of endoglin modulates TGF-beta1-signalling pathways in a novel immortalized mouse hepatic stellate cell line, PLoS One 8 (2013) e56116.

[40] E. Morris, I. Chrobak, A. Bujor, F. Hant, C. Mummery, P. Ten Dijke, M. Trojanowska, Endoglin promotes TGF-beta/Smad1 signaling in scleroderma fibroblasts, J. Cell. Physiol. 226 (2011) 3340-3348.

[41] L.D. Truong, G. Petrusevska, G. Yang, T. Gurpinar, S. Shappell, J. Lechago, D. Rouse, W.N. Suki, Cell apoptosis and proliferation in experimental chronic obstructive uropathy, Kidney Int. 50 (1996) 200-207.

[42] V.S. LeBleu, G. Taduri, J. O'Connell, Y. Teng, V.G. Cooke, C. Woda, H. Sugimoto, R. Kalluri, Origin and function of myofibroblasts in kidney fibrosis, Nat. Med. 19 (2013) 1047-1053.

[43] M.T. Grande, B. Sanchez-Laorden, C. Lopez-Blau, C.A. De Frutos, A. Boutet, M. Arevalo, R.G. Rowe, S.J. Weiss, J.M. Lopez-Novoa, M.A. Nieto, Snail1-induced partial epithelial-to-mesenchymal transition drives renal fibrosis in mice and can be targeted to reverse established disease, Nat. Med. 21 (2015) 989-997.

[44] M. Zeisberg, R. Kalluri, Cellular mechanisms of tissue fibrosis. 1. Common and organ-specific mechanisms associated with tissue fibrosis, American journal of physiology, Cell. Physiol. 304 (2013) C216-C225.

[45] M.A. Alikhan, S.D. Ricardo, Mononuclear phagocyte system in kidney disease and repair, Nephrology (Carlton) 18 (2013) 81-91.

[46] J.A. Moon, H.T. Kim, I.S. Cho, Y.Y. Sheen, D.K. Kim, IN-1130, a novel transforming growth factor-beta type I receptor kinase (ALK5) inhibitor, suppresses renal fibrosis in obstructive nephropathy, Kidney Int. 70 (2006) 1234-1243.

[47] M. Sato, Y. Muragaki, S. Saika, A.B. Roberts, A. Ooshima, Targeted disruption of TGF-beta1/Smad3 signaling protects against renal tubulointerstitial fibrosis induced by unilateral ureteral obstruction, J. Clin. Invest. 112 (2003) 1486-1494.

[48] X.M. Meng, X.R. Huang, A.C. Chung, W. Qin, X. Shao, P. Igarashi, W. Ju, E.P. Bottinger, H.Y. Lan, Smad2 protects against TGF-beta/Smad3-mediated renal fibrosis, J. Am. Soc. Nephrol. 21 (2010) 1477–1487.

[49] X.M. Meng, X.R. Huang, J. Xiao, A.C. Chung, W. Qin, H.Y. Chen, H.Y. Lan, Disruption of Smad4 impairs TGF-beta/Smad3 and Smad7 transcriptional regulation during renal inflammation and fibrosis in vivo and in vitro, Kidney Int. 81 (2012) 266-279.

[50] J.M. Munoz-Felix, J.M. Lopez-Novoa, C. Martinez-Salgado, Heterozygous disruption of activin receptor-like kinase 1 is associated with increased renal fibrosis in a mouse model of obstructive nephropathy, Kidney Int. 85 (2014) 319-332.

[51] M. Zeisberg, J. Hanai, H. Sugimoto, T. Mammoto, D. Charytan, F. Strutz, R. Kalluri, BMP-7 counteracts TGF-beta1-induced epithelial-to-mesenchymal transition and reverses chronic renal injury, Nat. Med. 9 (2003) 964-968.

[52] S.R. Manson, R.A. Niederhoff, K.A. Hruska, P.F. Austin, The BMP-7-Smad1/5/8 pathway promotes kidney repair after obstruction induced renal injury, J. Urol. 185 (2011) 2523–2530.

[53] J. Pannu, S. Nakerakanti, E. Smith, P. ten Dijke, M. Trojanowska, Transforming growth factor-beta receptor type I-dependent fibrogenic gene program is mediated via activation of Smad1 and ERK1/2 pathways, J. Biol. Chem. 282 (2007) 10405–10413.

[54] E. Wiercinska, L. Wickert, B. Denecke, H.M. Said, J. Hamzavi, A.M. Gressner, M. Thorikay, P. ten Dijke, P.R. Mertens, K. Breitkopf, S. Dooley, Id1 is a critical mediator in TGF-beta-induced transdifferentiation of rat hepatic stellate cells, Hepatology 43 (2006) 1032–1041.

[55] T. Matsubara, H. Abe, H. Arai, K. Nagai, A. Mima, H. Kanamori, E. Sumi, T. Takahashi, M. Matsuura, N. Iehara, A. Fukatsu, T. Kita, T. Doi, Expression of Smad1 is directly associated with mesangial matrix expansion in rat diabetic nephropathy, Lab. Investig. 86 (2006) 357-368.

[56] J.M. Munoz-Felix, M. Gonzalez-Nunez, J.M. Lopez-Novoa, ALK1-Smad1/5 signaling pathway in fibrosis development: friend or foe? Cytokine Growth Factor Rev. 24 (2013) 523-537.

[57] F.C. Luft, Soluble endoglin (sEng) joins the soluble fms-like tyrosine kinase (sFlt) receptor as a preeclampsia molecule, Nephrol. Dial. Transplant. 21 (2006) 3052-3054.

[58] J.M. Lopez-Novoa, Soluble endoglin is an accurate predictor and a pathogenic molecule in preeclampsia, Nephrol. Dial. Transplant. 22 (2007) 712-714.

[59] S. Venkatesha, M. Toporsian, C. Lam, J. Hanai, T. Mammoto, Y.M. Kim, Y. Bdolah, K.H. Lim, H.T. Yuan, T.A. Libermann, I.E. Stillman, D. Roberts, P.A. D'Amore, F.H. Epstein, F.W. Sellke, R. Romero, V.P. Sukhatme, M. Letarte, S.A. Karumanchi, Soluble endoglin contributes to the pathogenesis of preeclampsia, Nat. Med. 12 (2006) 642-649.

[60] M. Guerrero-Esteo, T. Sanchez-Elsner, A. Letamendia, C. Bernabeu, Extracellular and cytoplasmic domains of endoglin interact with the transforming growth factor-beta receptors I and II, J. Biol. Chem. 277 (2002) 29197-29209.

[61] N.P. Barbara, J.L. Wrana, M. Letarte, Endoglin is an accessory protein that interacts. with the signaling receptor complex of multiple members of the transforming growth factor-beta superfamily, J. Biol. Chem. 274 (1999) 584-594.

[62] A.L. Gregory, G. Xu, V. Sotov, M. Letarte, Review: the enigmatic role of endoglin in the placenta, Placenta 35 (Suppl) (2014) S93-S99.

Table 1

Primary antibodies used in immunohistochemistry.

Antigen	Supplier	Catalog number	Host species	Dilution
Fibronectin	Sigma-Aldrich	F3648	Rabbit	1:100
Collagen type I	Chemicon International	Ab765p	Rabbit	1:100
α-SMA	Sigma-Aldrich	A2547	Mouse	1:1000
S100A4	Chemicon International	07-2274	Rabbit	1:100
Ki67	Master Diagnóstica	mAD-000310QD	Rabbit	1:100
CD68	R&D Systems	AF796	Goat	1:100
CD31	Santa Cruz	sc-1506	Goat	1:50
iNOS	Biotechnology Santa Cruz	sc-651	Rabbit	1:50

Table 2

Primary antibodies used in Western blot.

Antigen	Supplier	Catalog number	Host species	Dilution
Endoglin (human)	Santa Cruz Biotech.	sc-20632	Rabbit	1:1,000
Fibronectin	Chemicon Intern.	Ab2033	Rabbit	1:1,000
Collagen type I	Chemicon Intern.	Ab765p	Rabbit	1:1000
α-SMA	Sigma-Aldrich	A2547	Mouse	1:1,000
S100A4	Chemicon Intern.	07-2274	Rabbit	1:1,000
Smad1	Santa Cruz Biotech.	sc-7965	Mouse	1:1,000
Smad2/3	Cell Signaling Tech.	sc-6032	Goat	1:1,000
Phospho-Smad1	Abcam	Ab63439	Rabbit	1:1,000
Phospho-Smad2	Calbiochem	566,415	Rabbit	1:1,000
Phospho-Smad3	Cell Signaling Tech.	9520	Rabbit	1:1,000
ICAM-1	R&D Systems	AF796	Goat	1:1,000
VCAM-1	Santa Cruz Biotech.	sc-1504	Goat	1:1,000
COX-2	Santa Cruz Biotech.	sc-1745	Goat	1:1,000
GAPDH	Ambion Appl. Biosyst.	AM4300	Mouse	1:50,000
β-actin	Sigma-Aldrich	A5441	Mouse	1:1,000
ALK1	Abgent	AP7807a	Rabbit	1:1,000
ALK5	Santa Cruz Biotech.	sc-398	Rabbit	1:1,000

FIGURE LEGENDS

Figure 1. Characterization of transgenic mice expressing human S-endoglin and analysis of endoglin expression after UUO. (a) Scheme of the DNA construct used to generate transgenic mice expressing human S-endoglin. A 5.0-kb SalI/KpnI fragment, containing a CMV enhancer, an actin enhancer/promoter, a β-globin (BG) intron (fragment SalI/EcoRI), the endoglin leader sequence-LS, the hemagglutinin epitope-HA, the human S-endoglin cDNA (fragment EcoRI/EcoRI) and a β-globin polyadenylation site-polyA (fragment EcoRI/KpnI), was microinjected in the pronuclei of fertilized oocytes to generate S-ENG+ mice. The transcription start site (TSS) and the translation initiation of the open reading frame (ORF) are indicated in the scheme. (b) Expression of human S-endoglin protein in different tissues (heart, spleen, lung, kidney, liver) from S-ENG+ mice. Protein extracts were analyzed by Western blot using anti-endoglin and anti-HA antibodies. As a loading control, glyceraldehyde 3-phosphate dehydrogenase (GAPDH) was included. (c) Expression of human S-endoglin after UUO (15 days) in WT and S-ENG+ mice. (d) Effect of human S-endoglin overexpression in systolic arterial blood pressure (SABP) (d1). Effect of human S-endoglin overexpression in renal function: creatinine clearance (d2) and proteinuria (d3) parameters. (e) Plasma concentrations of human soluble endoglin (Sol-Eng) in WT and S-ENG+ mice. (f) Mouse total endoglin (Left panel) and mouse short endoglin (Right panel) mRNA relative expression in NO and O kidneys from WT mice and S-ENG+ mice subjected to UUO for 15 days, analyzed by qPCR.

Figure 2. Effect of S-endoglin overexpression on renal interstitial fibrosis after unilateral ureteral obstruction. (a) Representative images of haematoxylin-eosin (b) Masson's trichrome staining and (c) Sirius red staining in sham operated (SO), non-obstructed (NO) and obstructed (O) kidneys from WT and S-ENG+ mice. In O kidneys we observe the main features of obstructive nephropathy: tubular dilatation (arrows) and atrophy (arrowhead), infiltration of inflammatory cells and hypercellularity (circles), and extracellular matrix deposition (stars). Bar = 100 μm. (c) Representative images and morphometric quantification of Sirius red of area stained (mean ± SEM); n = 4 in each group of mice. *p b 0.05 vs. their respective SO kidneys. #p b 0.05 vs. O kidneys from WT mice.

Figure 3. Effect of S-endoglin overexpression on renal collagen I and fibronectin after ureteral obstruction. (a) Representative immunohistochemistry images for fibronectin and collagen I in SO, NO and O kidneys from WT and S-ENG+ mice. Bar = 50 μm. (b) Western blot analysis of fibronectin and collagen I protein amount in SO, NO and O kidneys from WT and S-ENG+ mice. Densitometry analysis is represented as the mean ± SEM of 5–7 experiments per group. *p b 0.05 vs. SO kidneys. #p b 0.05 vs. O kidneys from WT mice.

Figure 4. Effect of S-endoglin overexpression on myofibroblast number after ureteral obstruction. (a) Representative immunohistochemistry images for α-SMA in SO, NO and O kidneys from WT and S-ENG+ mice (bar = 50 μm), and corresponding quantification of α-SMA-positive stained area in SO, NO and O

kidneys from WT and S-ENG+ mice expressed in square microns. (b) Representative immunohistochemistry images for S100A4 in SO, NO and O kidneys from WT and S-ENG+ mice. Bar = 50 μm. (c) Western blot analysis of S100A4 protein amount in SO, NO and O kidneys from WT and S-ENG+ mice. Densitometry analysis is represented as the mean ± SEM of 5–7 experiments per group. *p b 0.05 vs. SO kidneys. #p b 0.05 vs. O kidneys from WT mice.

Figure 5. Effect of S-endoglin overexpression on renal cell proliferation after ureteral obstruction. (a) Representative immunohistochemistry images for Ki67 and quantification of Ki67 positive cells. Bar = 50 μm. (b) Quantification of total, tubular (arrows) and interstitial (arrowheads) Ki67 positive cells. (c) Western blot analysis of PCNA protein amount in SO, NO and O kidneys from WT and S-ENG+ mice. (d) Quantification of tubular lumen area in O kidneys from WT and S-ENG+ mice. Densitometry analysis is represented as the mean ± SEM ofthe 5–7 experiments performed per group. *p b 0.05 vs. SO kidneys. #p b 0.05 vs. O kidneys from WT mice.

Figure 6. Effect of S-endoglin overexpression on renal inflammation and cell adhesion proteins after ureteral obstruction. (a) Representative immunostaining images for CD68 (monocyte¬macrophage marker), and iNOS in SO, NO and O kidneys from WT and S-ENG+ mice. Bar = 20 μmin CD68 and 50 μm in iNOS images. (b) Western blot analysis of ICAM-1, VCAM-1 and COX-2 protein amount in SO, NO and O kidneys from WT and S-ENG+ mice. (c) Quantification of peritubular capillaries and representative pictures of CD31 staining in SO, NO and O kidneys from WT and S-ENG+ mice. Densitometry analysis is represented as the mean ± SEM of the 5–7 experiments performed per group. *p b 0.05 vs. SO kidneys. #p b 0.05 vs. O kidneys from WT mice.

Figure 7. S-endoglin overexpression on Smad2/3 phosphorylation after ureteral obstruction. (a) Phospho-Smad2/3 representative immunostaining in SO, NO and O kidneys from WT and S¬ENG+ mice. Bar = 50 μm and histogram representing number of nuclei positively stained for phospho-Smad2/3 per field in SO, NO and O kidneys from WT and S-ENG+ mice. Data is represented as mean ± SEM. (b) Western blot analysis of phospho-Smad2, phospho-Smad3 and total Smad2/3 protein levels in SO, NO and O kidneys from WT and S-ENG+ mice. Densitometry analysis is represented as the mean ± SEM of 5–7 experiments per group (*p b 0.05 vs. SO kidneys; #p b 0.05 vs. O kidneys from WT mice).

Figure 8. Effect of S-endoglin overexpression on Smad1/5/8 phosphorylation after ureteral obstruction. (a) Phospho-Smad1/5/8 representative immunostaining for phospho-Smad1/5/8 in SO, NO and O kidneys from WT and S-ENG+ mice (bar = 50 μm), Bar= 50 μm and histogram representing number of phospho-Smad1/5/8-positive nuclei per field in SO,NO and O kidneys from WT and S-ENG+ mice. Data is represented as mean ± SEM. (b) Western blot analysis of phospho-Smad1 and total Smad1 protein levels in SO, NO and O kidneys from WT and S-ENG+ mice. Densitometry analysis is represented as the mean ± SEM of 5–7 experiments per group. *p b 0.05 vs. SO kidneys; **p b 0.05 vs. kidneys from WT.

Figure 9. Schematic summary of the role of Endoglin isoforms in kidney fibrosis. L-endoglin and S-endoglin modulate differentially TGF-β1-induced renal fibrosis. L-endoglin promotes phosphorylation of Smad2/3 and Smad1/5/8 proteins and consequent induction of renal fibrosis and inflammation (left hand side) whereas S-endoglin blocks Smad2/3 and Smad1/5/8 phosphorylation and consequent induction of renal fibrosis and inflammation (right hand side). This suggests that the complete cytoplasmic tail of endoglin is essential to regulate renal fibrosis.

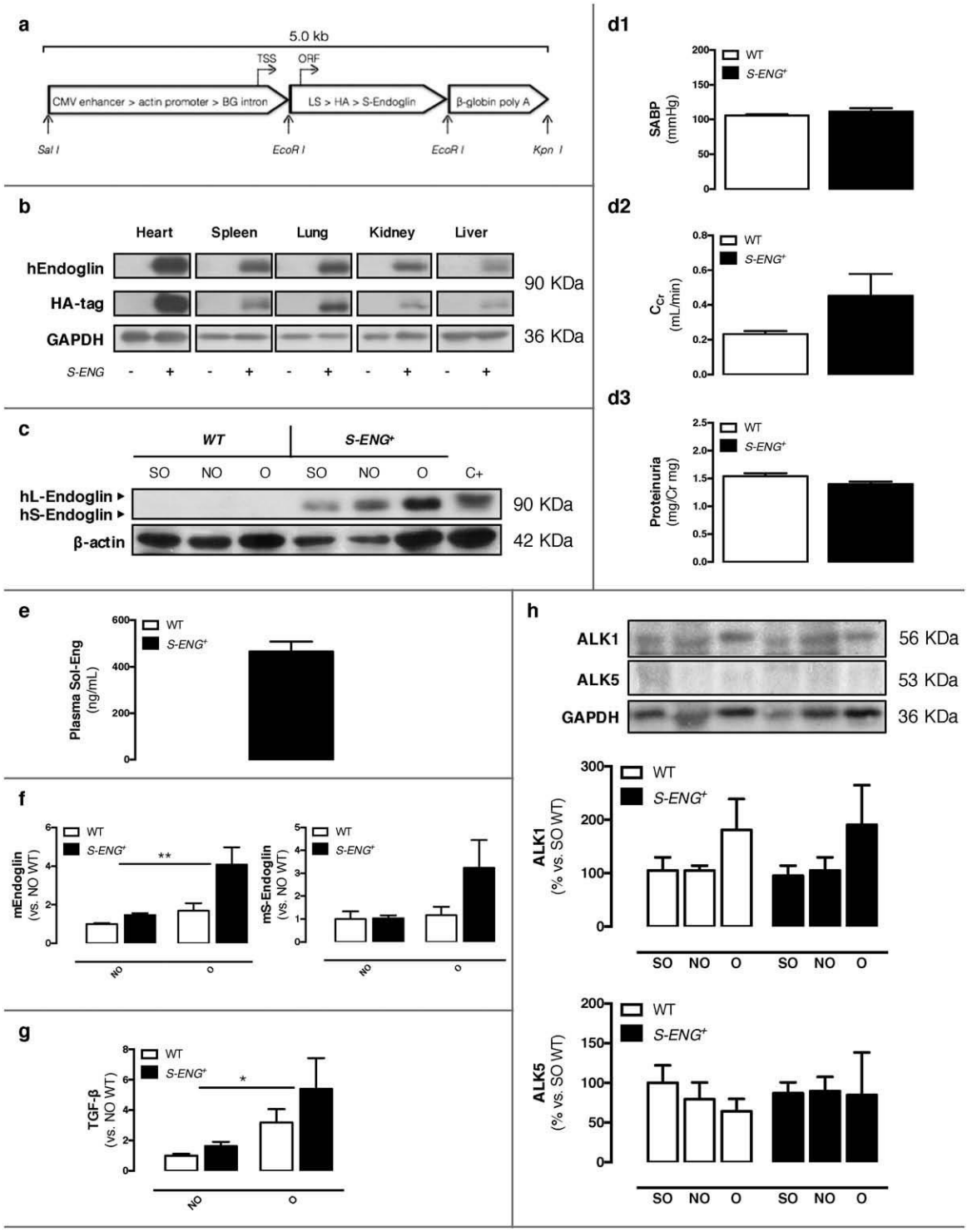
a
5.0 kb
TSS
ORF
CMV enhancer > actin promoter > BG intron
LS > HA > S-Endoglin
β-globin poly A
Sal I
EcoR I
EcoR I
Kpn I
b
Heart
Spleen
Lung
Kidney
Liver
hEndoglin
HA-tag
GAPDH
90 KDa
36 KDa
S-ENG - + - + - + - + - +
c
WT
S-ENG+
SO NO O SO NO O C+
hL-Endoglin
hS-Endoglin
β-actin
90 KDa
42 KDa
d1
SABP (mmHg)
WT
S-ENG+
d2
C_Cr (mL/min)
d3
Proteinuria (mg/Cr mg)
e
Plasma Sol-Eng (ng/mL)
f
mEndoglin (vs. NO WT)
mS-Endoglin (vs. NO WT)
**
NO
O
g
TGF-β (vs. NO WT)
*
h
ALK1
ALK5
GAPDH
56 KDa
53 KDa
36 KDa
ALK1 (% vs. SO WT)
ALK5 (% vs. SO WT)
SO NO O SO NO O

FIGURE 1

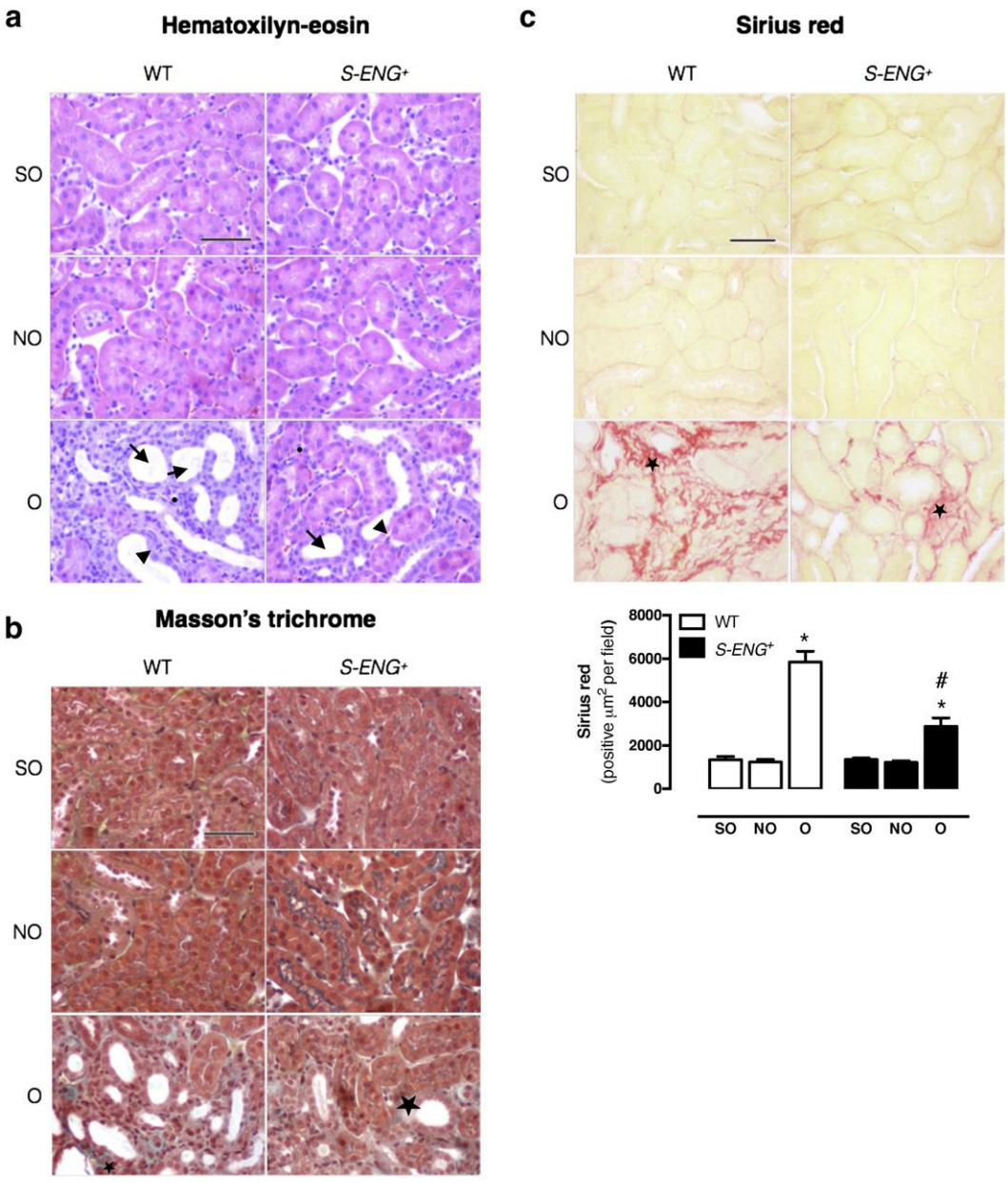
a
Hematoxilyn-eosin
WT
S-ENG+
SO
NO
O
b
Masson's trichrome
WT
S-ENG+
SO
NO
O
c
Sirius red
WT
S-ENG+
SO
NO
O
Sirius red
(positive μm² per field)
8000
6000
4000
2000
0
WT
S-ENG+
*
#
*
SO NO O SO NO O

FIGURE 2

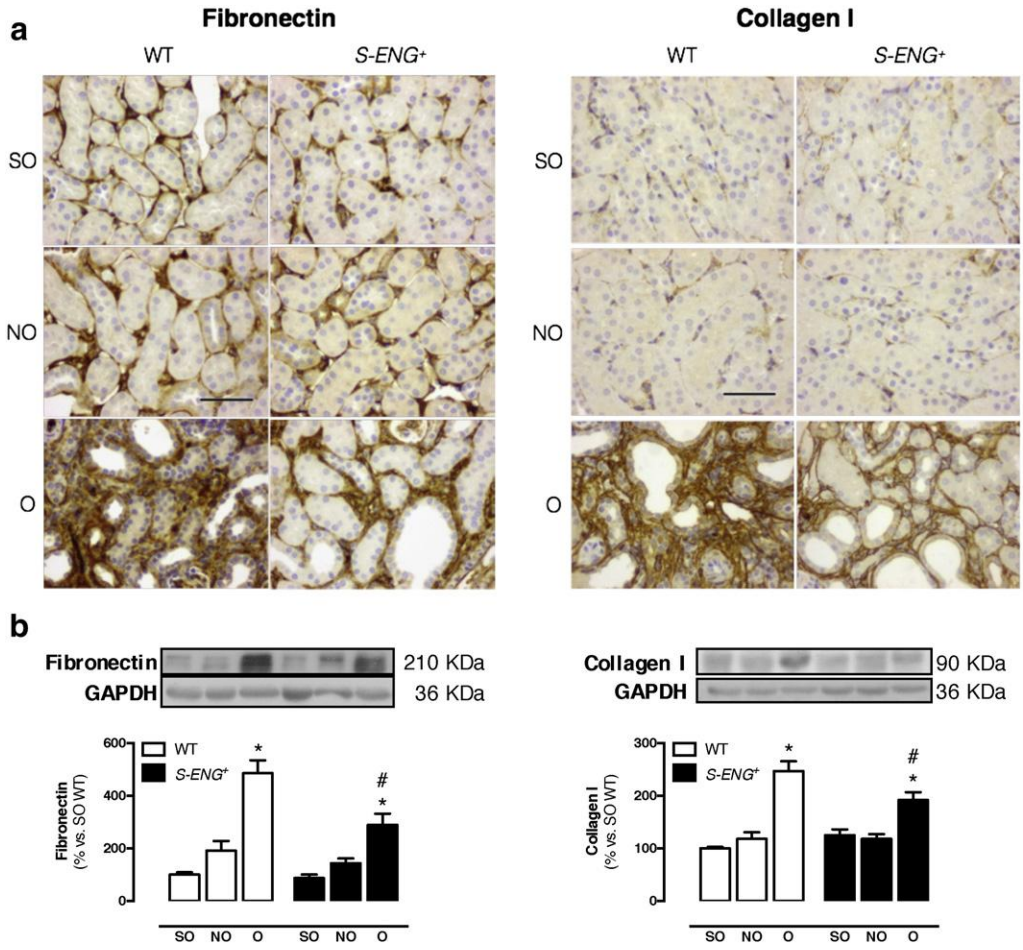
a
Fibronectin
Collagen I
WT
S-ENG+
SO
NO
O
b
Fibronectin
GAPDH
210 KDa
36 KDa
Collagen I
GAPDH
90 KDa
36 KDa
Fibronectin (% vs. SO WT)
Collagen I (% vs. SO WT)
SO NO O SO NO O

FIGURE 3

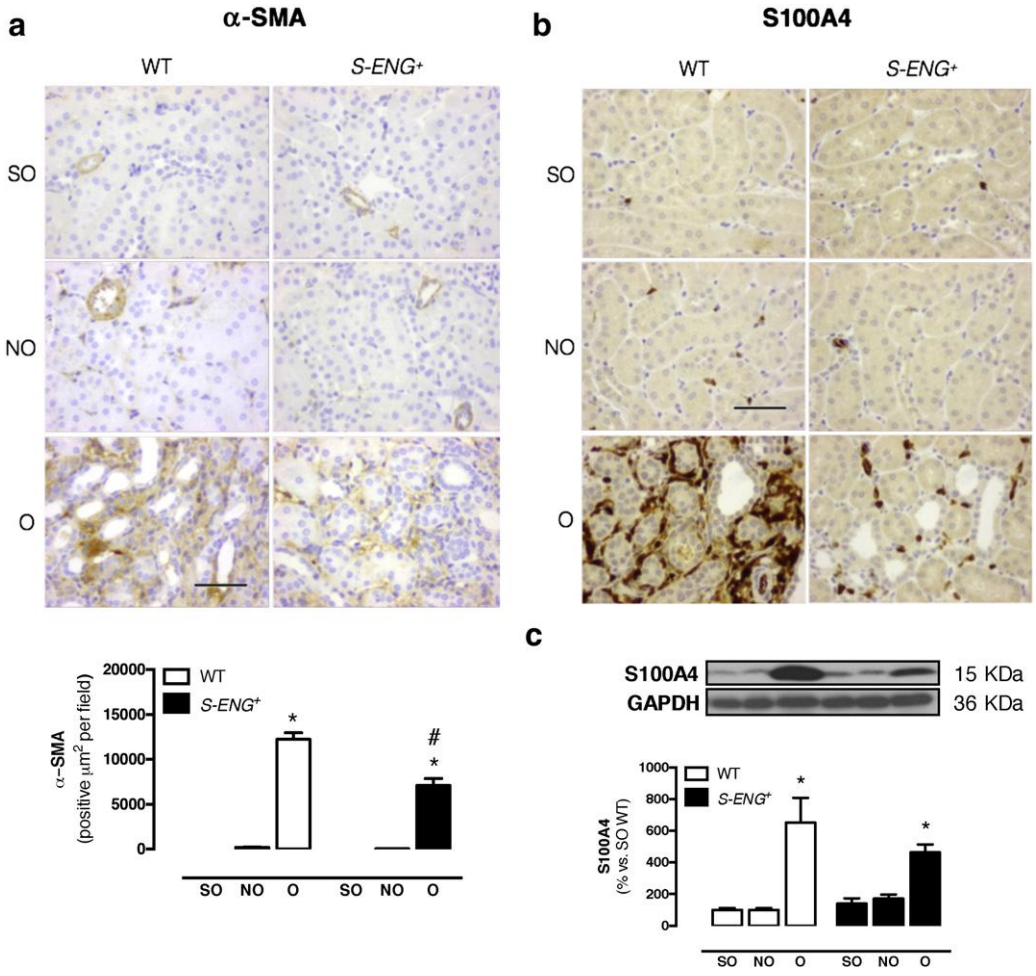
a
α-SMA
WT
S-ENG+
SO
NO
O
b
S100A4
WT
S-ENG+
SO
NO
O
c
S100A4
GAPDH
15 KDa
36 KDa
WT
S-ENG+
α-SMA (positive μm2 per field)
20000
15000
10000
5000
0
*
#
*
SO NO O SO NO O
WT
S-ENG+
S100A4 (% vs. SO WT)
1000
800
600
400
200
0
*
*
SO NO O SO NO O

FIGURE 4

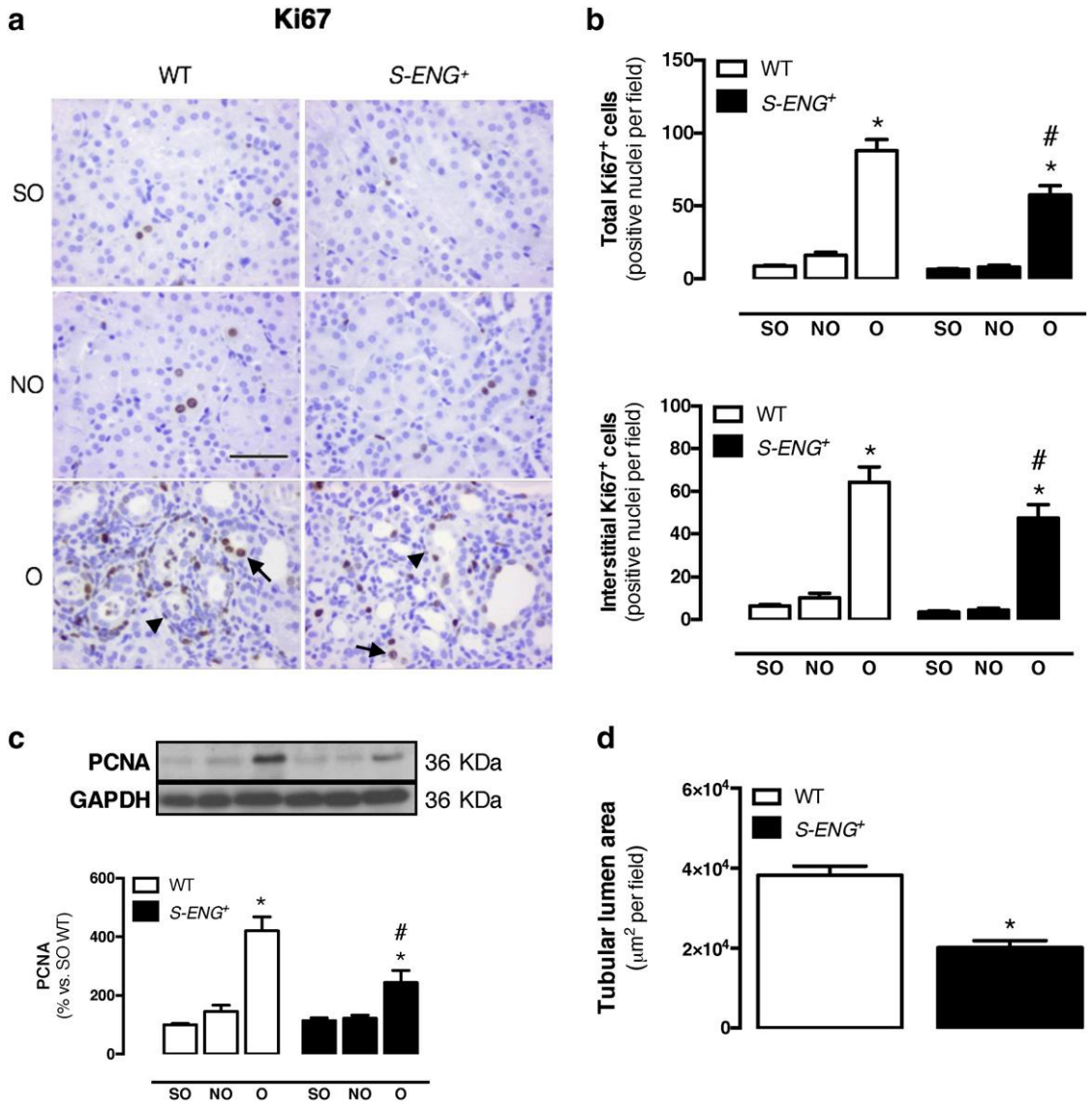
a
Ki67
WT
S-ENG+
SO
NO
O
b
Total Ki67+ cells
(positive nuclei per field)
WT
S-ENG+
150
100
50
0
SO NO O SO NO O
Interstitial Ki67+ cells
(positive nuclei per field)
100
80
60
40
20
0
c
PCNA
GAPDH
36 KDa
36 KDa
PCNA
(% vs. SO WT)
600
400
200
0
d
Tubular lumen area
(μm2 per field)
6x10^4
4x10^4
2x10^4
0

FIGURE 5

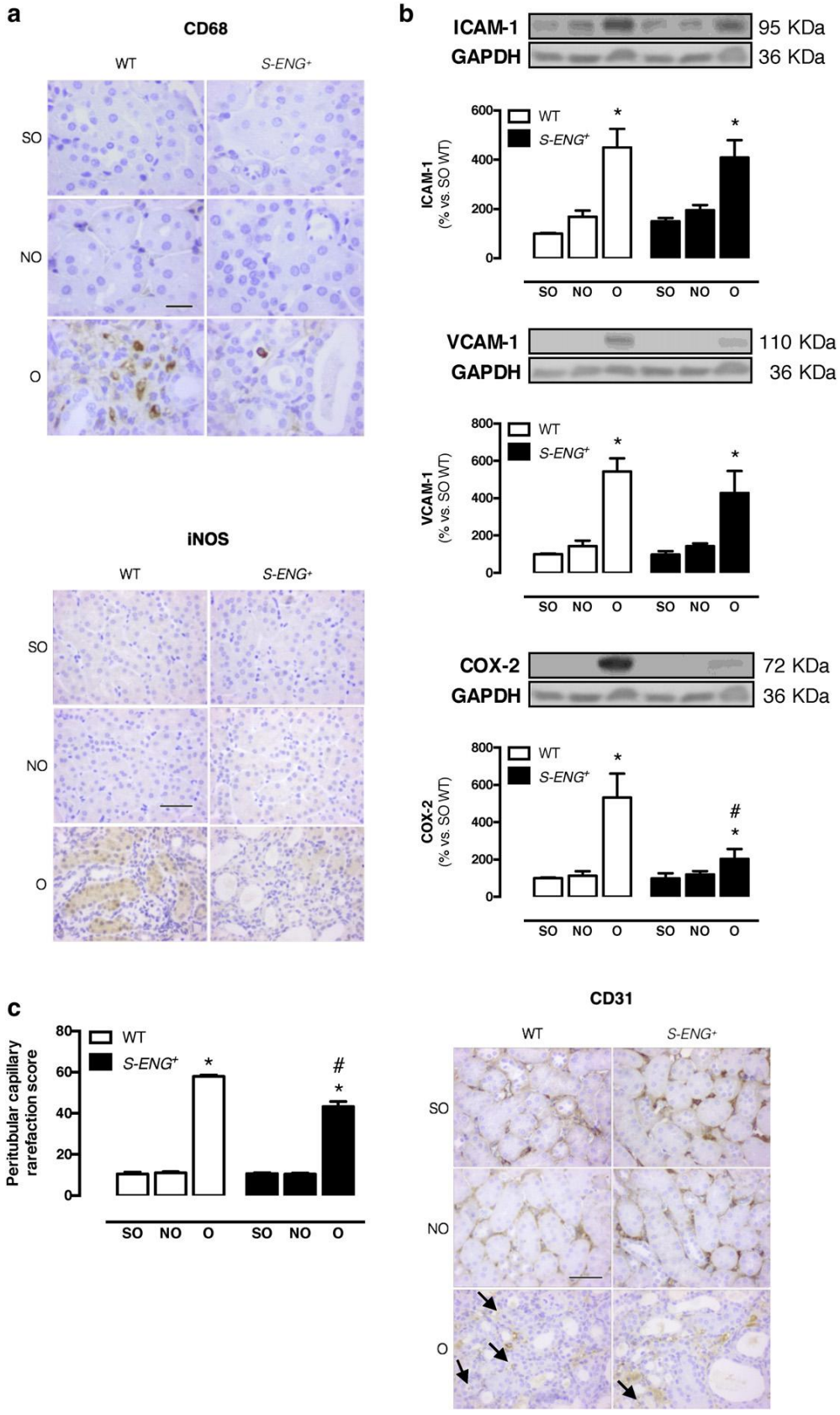
a
CD68
WT
S-ENG+
SO
NO
O
iNOS
WT
S-ENG+
SO
NO
O
b
ICAM-1
95 KDa
GAPDH
36 KDa
WT
S-ENG+
ICAM-1
(% vs. SO WT)
600
400
200
0
SO NO O SO NO O
VCAM-1
110 KDa
GAPDH
36 KDa
WT
S-ENG+
VCAM-1
(% vs. SO WT)
800
600
400
200
0
SO NO O SO NO O
COX-2
72 KDa
GAPDH
36 KDa
WT
S-ENG+
COX-2
(% vs. SO WT)
800
600
400
200
0
SO NO O SO NO O
c
Peritubular capillary rarefaction score
80
60
40
20
0
WT
S-ENG+
SO NO O SO NO O
CD31
WT
S-ENG+
SO
NO
O

FIGURE 6

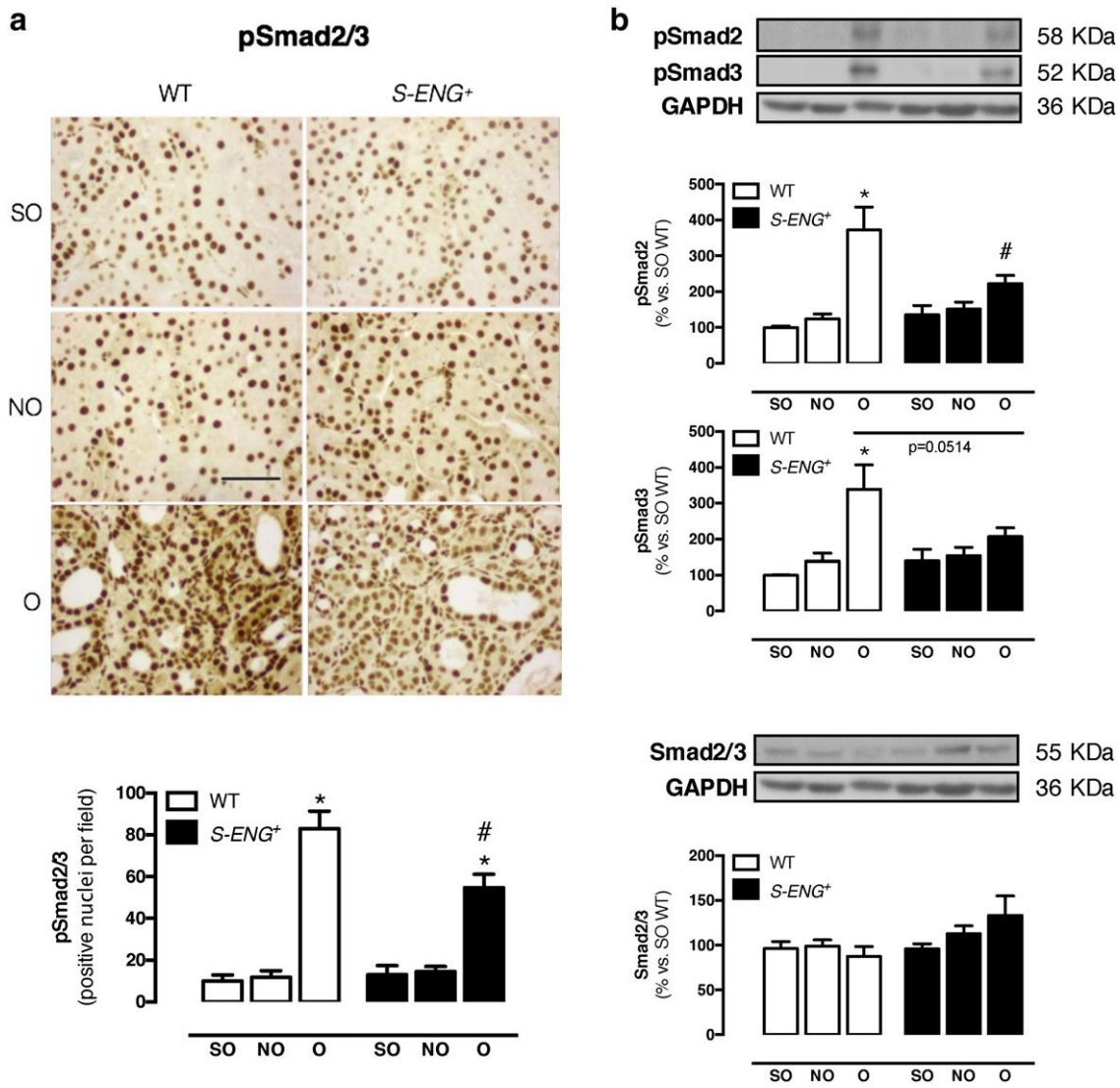
a
pSmad2/3
WT
S-ENG+
SO
NO
O
pSmad2/3
(positive nuclei per field)
WT
S-ENG+
SO NO O SO NO O
b
pSmad2
pSmad3
GAPDH
58 KDa
52 KDa
36 KDa
pSmad2
(% vs. SO WT)
pSmad3
(% vs. SO WT)
p=0.0514
Smad2/3
GAPDH
55 KDa
36 KDa
Smad2/3
(% vs. SO WT)

FIGURE 7

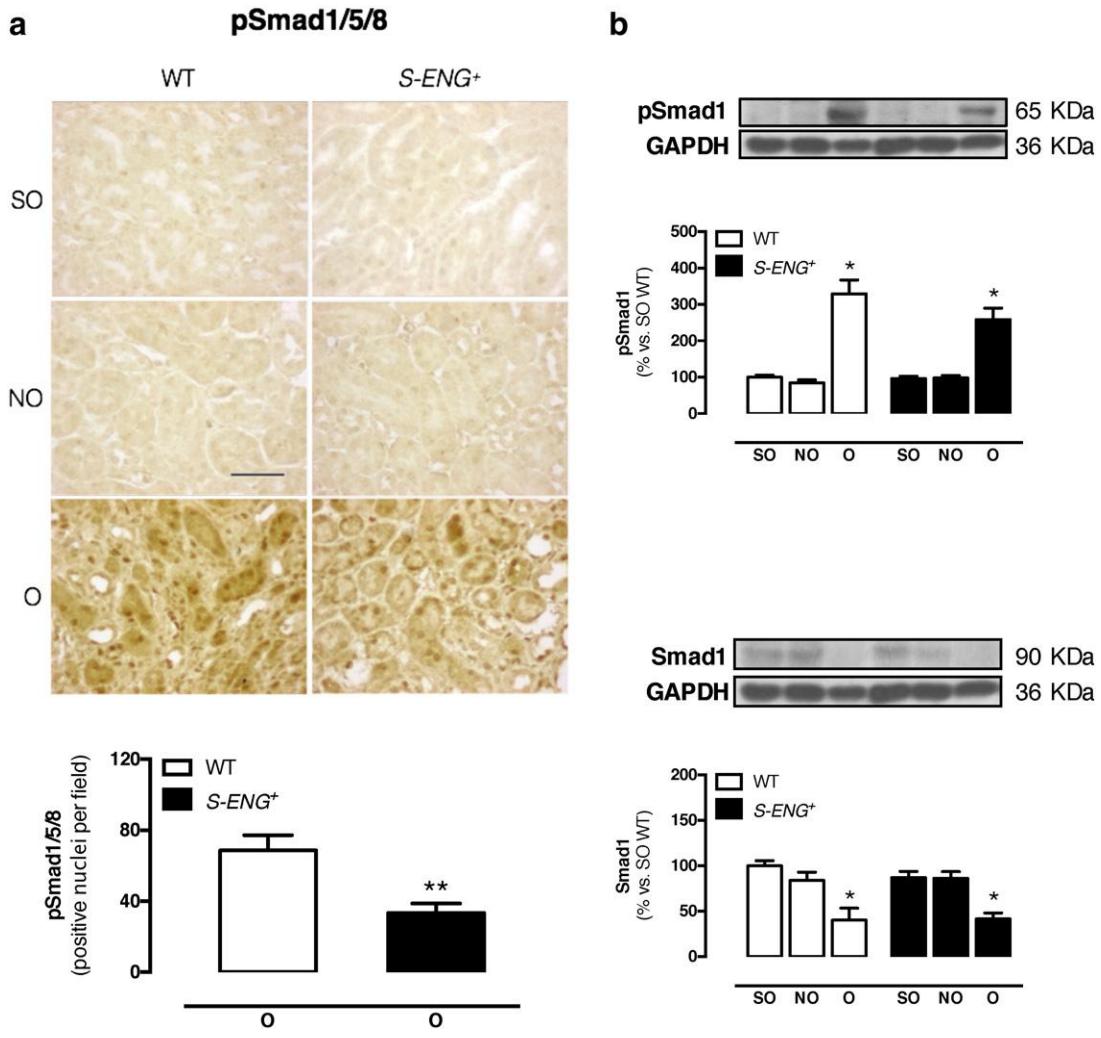
a
pSmad1/5/8
WT
S-ENG+
SO
NO
O
pSmad1/5/8 (positive nuclei per field)
120
80
40
0
WT
S-ENG+
**
O
O
b
pSmad1
GAPDH
65 KDa
36 KDa
pSmad1 (% vs. SO WT)
500
400
300
200
100
0
WT
S-ENG+
*
*
SO NO O SO NO O
Smad1
GAPDH
90 KDa
36 KDa
Smad1 (% vs. SO WT)
200
150
100
50
0
WT
S-ENG+
*
*
SO NO O SO NO O

FIGURE 8

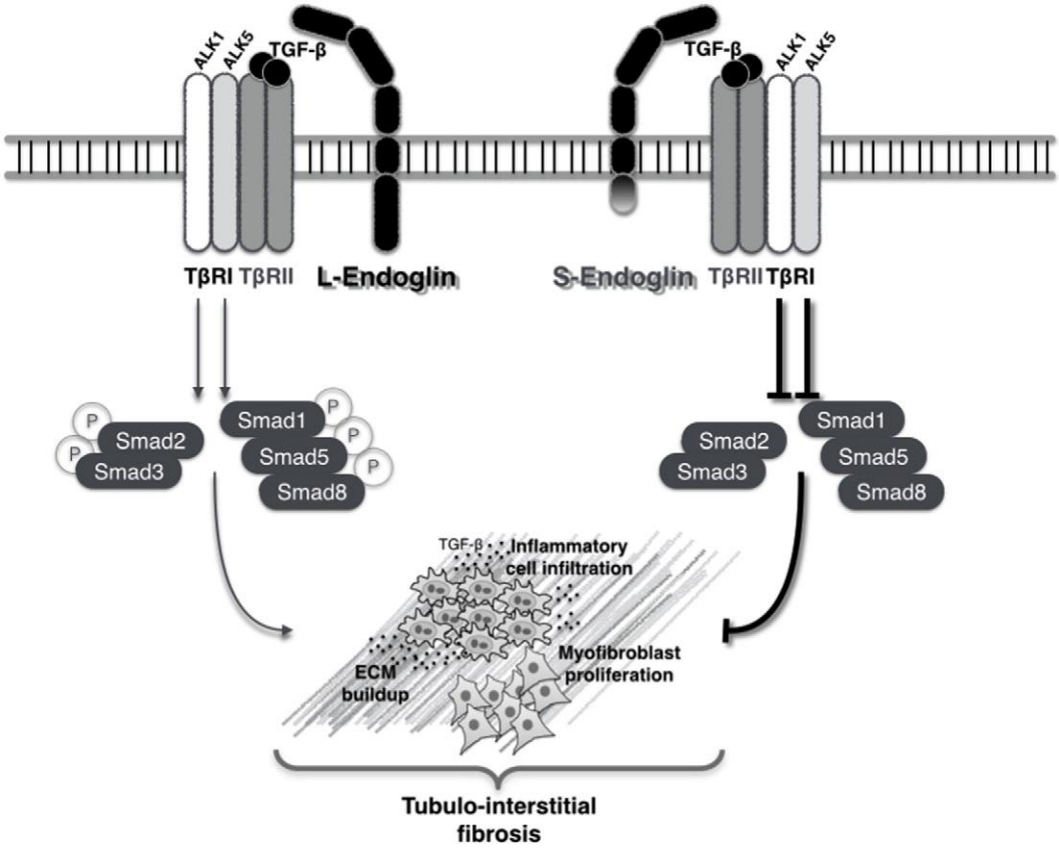
ALK1
ALK5
TGF-β
TGF-β
ALK1
ALK5
TβRI TβRII
L-Endoglin
S-Endoglin
TβRII TβRI
P
Smad2
Smad3
Smad1
Smad5
Smad8
Smad2
Smad3
Smad1
Smad5
Smad8
TGF-β
Inflammatory cell infiltration
Myofibroblast proliferation
ECM buildup
Tubulo-interstitial fibrosis

FIGURE 9